Korean J. Chem. Eng., 36(4), 584-590 (2019)
DOI: 10.1007/s11814-019-0235-9

pISSN: 0256-1115
eISSN: 1975-7220

Fabrication of tubular ceramic-supported malic acid cross-linked poly(vinyl alcohol)/ rice husk ash-silica nanocomposite membranes for ethanol dehydration by pervaporation

Tran Minh Ngoc*, Tran Minh Man*, Mai Thanh Phong, Hoang Minh Nam*,**, and Nguyen Huu Hieu*,**,†**

*Key Laboratory of Chemical Engineering and Petroleum Processing, Ho Chi Minh City University of Technology - Vietnam National University (HCMUT - VNU), Ho Chi Minh City 700000, Vietnam
**Faculty of Chemical Engineering, HCMUT - VNU, Ho Chi Minh City 700000, Vietnam
(*Received 4 November 2018 • accepted 19 January 2019*)

Abstract−Silica nanoparticles were prepared from rice husk ash (RHA-silica) by precipitation method. The characterization of RHA-silica was studied by X-ray fluorescence, X-ray diffraction (XRD), Fourier transform infrared spectroscopy (FTIR), transmission electron microscopy, and Brunauer-Emmett-Teller specific surface area. Results showed that RHA-silica was successfully synthesized with a particle size of 5-15 nm and purity of 98.08%. The obtained RHA-silica was applied with different content for fabrication of tubular ceramic-supported poly(vinyl alcohol) membranes using malic acid as a cross-linking agent (RHA-silica/MA-PVA) by dip-coating and solvent evaporation methods. The tubular ceramic-supported RHA-silica/MA-PVA membranes were used for dehydration of 95 wt% ethanol solution by pervaporation (PV) technology. Results indicated membrane with 15 wt% RHA-silica (15RHA-silica/MA-PVA) was suitable for the dehydration with permeate flux of 0.0856 kg/m^2·h, separation factor of 46.6, and pervaporation separation index of 3.9 kg/m^{2}h. The tubular ceramic-supported 15RHA-silica/MA-PVA membrane was characterized using XRD, FTIR, scanning electron microscope, differential scanning calorimetry, and contact angle measurement. Results showed that this membrane was 30 μm thick, mechanical stable (swelling rate, 133.9%), hydrophobic (contact angle, 81°), and thermal stable (glass transition temperature, 138.7 °C). Therefore, the tubular ceramic-supported nanocomposite membrane could be considered as a potential alternative for PV dehydration of ethanol.

Keywords: RHA-silica, Poly(vinyl alcohol), Nanocomposite, Tubular Membrane, Dehydration, Pervaporation

INTRODUCTION

Ethanol as a renewable source of energy can be an alternative to traditional fuels. Due to high-energy values, adding a small amount of ethanol to gasoline increases the combustion efficiency. Besides, the use of ethanol reduces the emission of exhaust fumes and helps to protect the environment. To be used as a source of fuel, ethanol with purity higher than 99 wt% is required. Several methods to increase the purity of ethanol have been developed, such as azeotropic distillation, extractive distillation vapor permeation, pervaporation, and adsorption on molecular sieves [1]. However, distillation method faces difficulty in separating ethanol from ethanol/water azeotrope mixture. Other techniques are uneconomical due to high investment cost.

In recent years, pervaporation (PV) has been considered as a suitable separation technology for ethanol dehydration, which has attracted attention from a number of researchers [2]. PV is a membrane separation process in which the components of a liquid mixture are separated by partial vaporization through a dense non-porous membrane.

In the PV process, the driving force for mass transfer is the difference in partial vapor pressure between two sides of the membrane, as shown in Fig. 1 [3,4]. Moreover, no extra reagents are needed in the PV process compared to azeotropic and extractive distillation. Thus, this process is an environment-friendly and energy-efficient separation technology. The separation efficiency of PV process depends on the membrane properties and operating conditions.

Poly(viny alcohol) (PVA) is one of the most common materials for synthesis of membranes used in the dehydration of ethanol be-

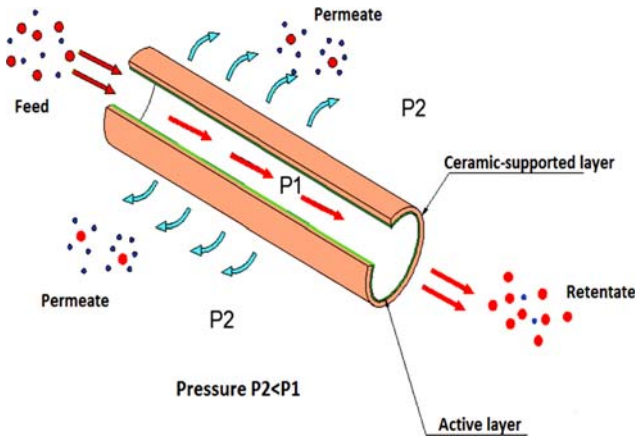

Fig. 1. Structure and working principle of tubular nanocomposite membrane.

†To whom correspondence should be addressed.
E-mail: nhhieubk@hcmut.edu.vn

cause of its high chemical stability, low manufacturing cost, excellent film-forming ability, and high hydrophilicity. However, the application of PVA in PV is restricted due to its water solubility, swelling in water, and instability at high temperature operation [5,6]. To overcome these disadvantages, cross-linking agents and fillers are added to PVA membranes.

Compared with several common cross-linking agents such as glutaraldehyde, maleic acid, and fumaric acid, malic acid (MA) is more hydrophilic and has smaller structure, which enhances interactions with PVA. Furthermore, permeate flux through MA-PVA membrane is better than neat PVA membrane. The suitable MA content is 20 wt% with respect to the weight of PVA based on the previous researches [7,8].

Many types of filler have been used in preparation of composite membranes to increase PV performance, such as zeolite, silica, metal-organic frameworks, and graphene. Among them, silica, which contains silanol groups (-Si-OH), can form hydrogen bonds with hydroxyl groups on PVA surface. This creates a rigid polymer matrix, leading to the increase in membrane performance (permeate flux, selectivity, and pervaporation separation index) and characteristics (swelling rate, contact angle, and glass transition temperature) [9,10].

To increase the membrane permeability, a tubular module with an active layer of membrane on a porous ceramic support has been developed. The structure and working principle of tubular membrane are illustrated in Fig. 1. The tubular membrane has many advantages, including good anti-sludge, large effective area, mechanical and chemical stability, and feasibility to be applied in industrial scale [11].

Previous researches applied fumed silica in modifying membranes for PV. In this study, silica nanoparticles were synthesized from rice husk ash (RHA-silica) by precipitation method. Effect of RHA-silica content on PV performance to dehydration of 95 wt% ethanol solution of tubular ceramic-supported malic acid-poly(vinyl alcohol) (RHA-silica/MA-PVA) membranes was investigated. The characterization of suitable RHA-silica/MA-PVA membrane was studied by X-ray diffraction (XRD), Fourier transform infrared spectroscopy (FTIR), scanning electron microscope (SEM), swelling rate, contact angle measurement, and differential scanning calorimetry (DSC).

MATERIALS AND METHODS

1. Materials

RHA was supplied from Thanh Binh brickyard, Dong Thap Province, Vietnam. Ceramic tubes were fabricated at Faculty of Materials Technology, Ho Chi Minh City University of Technology. Sodium hydroxide (98 wt%), hydrochloric acid (36 wt%), PVA (molecular weight, 160,000 g/mol, degree of hydrolysis, 86.5-89%), and MA (99 wt%) were purchased from Xilong Chemical, China. Ethanol (95 wt%) was purchased from Vina Chemsol, Vietnam. All chemicals were of analytical reagent standard, and double-distilled water was used in all experiments.

2. Preparation of RHA-silica

Silica nanoparticles were prepared from RHA-silica by precipitation method [12]. 10 g of RHA was pretreated with 250 mL of 1 N HCl solution by stirring for 30 min at 40 °C. Then, the mixture was filtered by a vacuum filter system. The obtained solid was washed with distilled water to partially remove the excess acid. Next, 10 g of pretreated RHA was stirred in 250 mL of 2 N NaOH solution. The mixture was boiled at 90 °C for 2 h before being filtered by a vacuum filter system. Then, the filtrate was cooled to room temperature, and 1 N HCl solution was added until pH reached the value of 7 under stirring condition. The forming precipitation was washed and centrifuged with distilled water and ethanol, respectively. The final product was dried at 100 °C, then ground to homogeneous powder.

3. Preparation of Tubular Ceramic-supported RHA-silica/MA-PVA Membranes

The tubular ceramic-supported RHA-silica/MA-PVA membranes were prepared by dip-coating and solvent evaporation methods [13]. Ceramic tubes were dried at 100 °C for 30 min. First, 5 g of PVA was dissolved in 300 mL of distilled water at 80 °C. Next, 1 g of MA was added into the PVA solution, as described elsewhere [8]. RHA-silica (0, 5, 10, 15, and 20 wt% with respect to PVA weight) was gradually added into MA-PVA solution. Membranes were marked as 0RHA-silica/MA-PVA, 5RHA-silica/MA-PVA, 10RHA-silica/MA-PVA, 15RHA-silica/MA-PVA, 20RHA-silica/MA-PVA corresponding to RHA-silica content. The inside of the ceramic tube was dip-coated with RHA-silica/MA-PVA solution for ten minutes and dried at 100 °C. Finally, the tubular composite membranes were dried at 120 °C for 3 h.

4. Pervaporation Experiments

The PV system used in this study is illustrated in Fig. 2. The PV dehydration of ethanol was as follows: 1.5 L of 95 wt% ethanol solution was fed into the feed tank, recirculated by centrifugal pump and heated to 50 °C by heating coil. RHA-silica/MA-PVA membrane was put into the tubular module. All experiments were carried out in 2 h and the flow rate was fixed at 60 L/h. The vacuum pressure on the permeate side was kept at 100 kPa by vacuum pump. The permeate solution obtained from the cold trap was weighed and the alcohol content was identified by a refractometer to determine the selectivity. Permeate flux (J), selectivity (α) and PV separation index (PSI) are calculated as follows:

$$J = \frac{\Delta W}{A \times \Delta t} \quad (1)$$

where J is the permeate flux (kg/m^{2}h), ΔW is the mass of permeate (kg), A is the effective membranes area (m^2), and Δt is the permeation time (hour).

$$\alpha = \frac{y_{H_2O}/y_{C_2H_5OH}}{x_{H_2O}/x_{CH_3OH}} \quad (2)$$

where x and y are the mass fractions of either water or ethanol in the feed and permeate, respectively.

$$PSI = J(\alpha - 1) \quad (3)$$

5. Characterization

The components of RHA-silica were analyzed by X-ray fluorescence (XRF) (Bruker-S2 Range) at 50 W, 50 kV, 2 mA of X-ray power directly. XRD patterns were obtained by D8-ADVANCE with the voltage of 40 kV and electric current of 40 mA, K=1.54184 Å. FTIR spectra were analyzed with wave number from 4,000 to 500 cm^{-1}

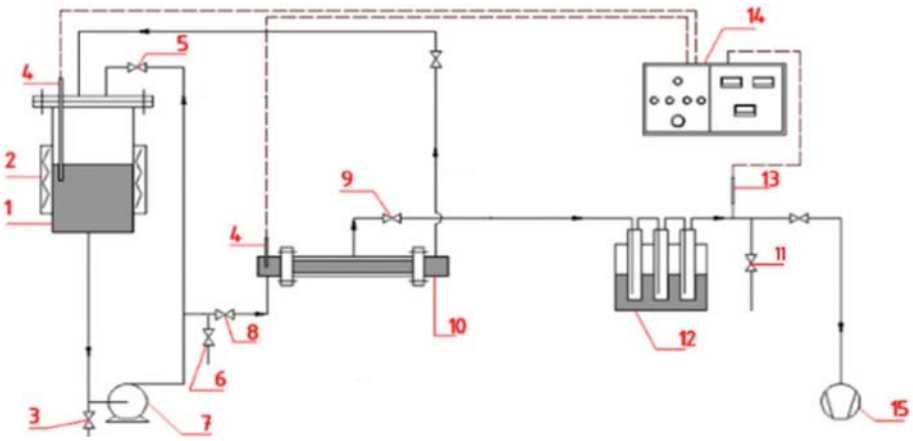

Fig. 2. Schematic diagram of tubular membrane module PV system.

1. Feed tank	5. Recirculation valve	9. Permeate valve	13. Vacuum gauge
2. Heating coil	6. Sample valve	10. Single tubular membrane module	14. Process control panel
3. Drain valve	7. Feed pump	11. Vacuum relief valve	15. Vacuum pump
4. Thermometer	8. Flow rate control valve	12. Cold trap	

during 64 scans on Alpha-E Bruker (Bruker Optik GmbH, Ettlingen, Germany) spectrometer. DSC was performed with Mettler Toledo, heating step 10 °C/min, amplitudes of 0-250 °C. TEM images were taken by JEM-1400 machine with an accelerating voltage of 100 kV. SEM images were taken by JSM 7401F-ICT-VAST. Brunauer-Emmett-Teller (BET) specific surface area of RHA-silica was determined by the nitrogen adsorption according to B.E.T method (Quantachrome, NOVA 2200e, USA). Contact angles of membranes with water were measured using SCA20. Membrane was dipped in pure water for 1 day and swelling rate (SR) was calculated as follows:

$$SR = \frac{W_m - D_m}{D_m} 100\% \quad (4)$$

where W_m (g) is the wet mass of the membrane, D_m (g) is the dry mass of the membrane. All measurements were under the following conditions: 25 °C and relative humidity of 30%.

RESULTS AND DISCUSSION

1. RHA-silica Characterization

1-1. XRF Analysis

RHA-silica product is shown in Fig. 3. The purity of silica in RHA-silica is higher than pyrolysis method (95% RHA-silica) [13] and base-acid method (98% RHA-silica) [14] as shown in Table 1. Other oxides have low remaining content. Therefore, the obtained RHA-silica with high purity is suitable for membrane fabrication as a filler.

1-2. XRD Analysis

XRD pattern of RHA-silica is shown in Fig. 4. As can be seen, a strong broad peak between 20° and 30° (2θ=24°) is typical of amorphous silica, as described in previous research [15].

1-3. FTIR Analysis

FTIR spectrum of RHA-silica is shown in Fig. 5. As can be seen, a broad band appears between 2,800 cm^{-1} and 3,750 cm^{-1} corresponding to the stretching vibration of -Si-OH groups. The peak at 1,645 cm^{-1} corresponds to the -OH stretching vibration of the absorbed water. The predominant absorbance peak at 1,091 cm^{-1} is

Fig. 3. RHA-silica product.

Table 1. Composition of oxides in synthesized RHA-silica

Composition	Mass, %
SiO_2	98.08
Na_2O	0.60
Al_2O_3	0.76
SO_3	0.34
P_2O_5	0.03
Fe_2O_3	0.01
Sb_2O_3	0.05
CdO	0.04
SnO_2	0.06

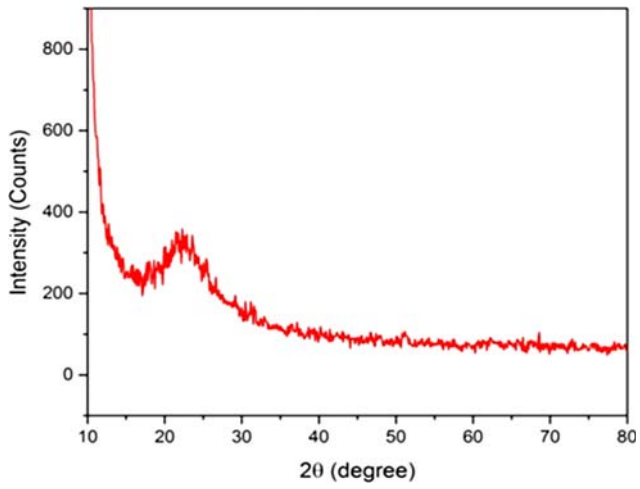

Fig. 4. XRD pattern of RHA-silica.

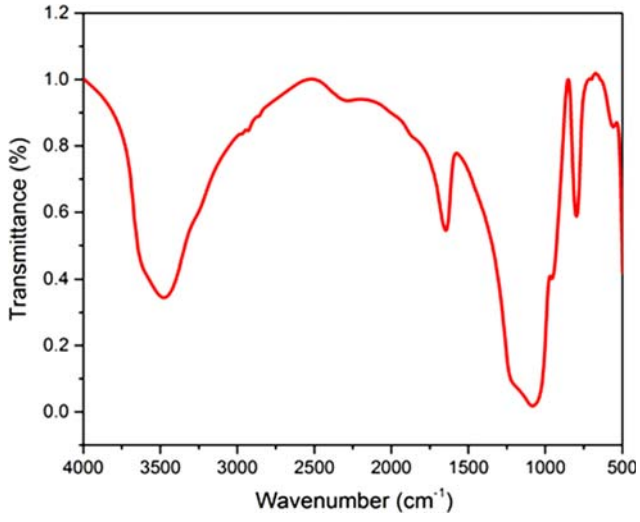

Fig. 5. FTIR spectrum of RHA-silica.

assigned to the vibrations of siloxane groups (Si-O-Si). These peaks in the spectrum of RHA-silica confirm the presence of typical bonds in RHA-silica structure [16]. This result indicated that RHA-silica was successfully synthesized.

1-4. TEM Images

Fig. 6 shows TEM images of RHA-silica. RHA-silica particles have an average size in range of 5 to 15 nm. Furthermore, RHA-silica particles tend to aggregate because of the interaction among -OH groups of silanol groups on particle surface to form Si-O-Si bond between silica particles during solvent elimination by drying [17].

1-5. BET Specific Surface Area

BET specific surface area of RHA-silica is 290.724 m^2/g. This result is higher than the BET specific surface area of RHA-silica synthesized by pyrolysis method. This could be explained by the fact that in pyrolysis method, RHA is heated at high temperature for a long time, causing an agglomeration effect, diminishing porosity [18].

2. Effect of RHA-silica Content on PV Performance of Tubular Ceramic-supported RHA-silica/MA-PVA Membranes

As shown in Fig. 7(a), when the content of RHA-silica is less than

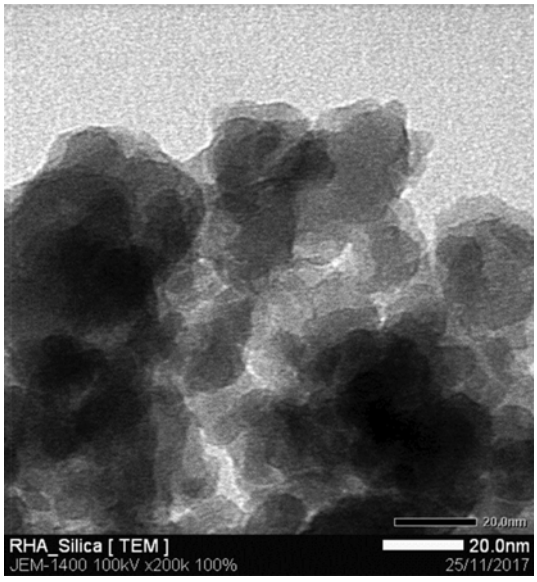

Fig. 6. TEM images of RHA-silica.

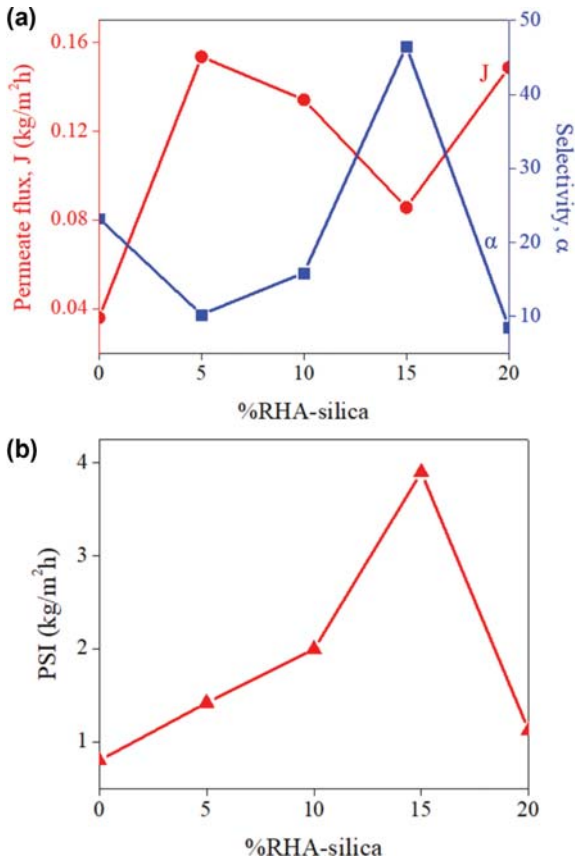

Fig. 7. Effect of RHA-silica content on PV performance of RHA-silica/MA-PVA membrane. (a) Permeate flux and separation factor, (b) PSI.

5 wt%, the permeate flux increases and separation factor decreases. Permeate flux decreases and separation factor increases when the content of RHA-silica is increased from 5 to 15 wt%. When RHA-silica content is higher than 15 wt%, permeate flux increases and

separation factor decreases again. Fig. 7(b) shows the highest pervaporation index is 3.9 kg/m^{2}h at the RHA-silica content of 15 wt%. This result could be due to the really low number of -Si-OH groups at low RHA-silica content (<5 wt%). Thus, the hydrogen bonds between RHA-silica and PVA are hardly formed. Furthermore, the appearance of RHA-silica particles increases the free-volume in PVA polymer matrix. Those cause the expansion of polymer matrix, leading to an increase in permeate flux and a decrease in separation factor. At higher RHA-silica content (>5 wt%), the number of -Si-OH groups is higher and hydrogen bonds are formed between -Si-OH in RHA-silica and -OH in PVA, leading to rigid polymer matrix formation. Thus, the membranes show a decrease in permeability and an increase in selectivity. When the RHA-silica content is higher than 15 wt%, RHA-silica particles tend to form aggregation due to the increase in hydrogen bonding and the interactions between PVA and RHA-particle become weak. The aggregation of RHA-silica also forms boundary defects on the RHA-silica and membrane boundaries, leading to an increase in free-volume in polymer matrix. Thus, the permeability increases and the selectivity decreases [15]. Therefore, 15RHA-silica/MA-PVA membrane was suitable for ethanol dehydration.

3. Membrane Characterization

3-1. XRD Analysis

XRD patterns of neat PVA and 15RHA-silica/MA-PVA are shown in Fig. 8. The XRD pattern of 15RHA-silica/MA-PVA has a characteristic peak of PVA at 2θ=18° [19]. The typical peak at 2θ=21° of amorphous silica is not observed, indicating the good dispersion of silica particles in PVA matrix. The interactions between -OH groups on the surface of RHA-silica particles and PVA result in the increase in crystallinity and decrease in holes in polymer matrix. The increase in crystallinity leads to the decrease in permeability and increase in selectivity of the membrane. This is because the crystallinity limits the entering of feed solution constituents into PVA structure [20]. This result is consistent with the PV experimental data.

3-2. FTIR Analysis

FTIR spectra of neat PVA, MA-PVA, and 15RHA-silica/MA-PVA membranes are shown in Fig. 9. The neat PVA membrane (Fig. 9(a)) shows a broad band between 3,750 and 3,200 cm^{-1} due to the -OH stretching vibration. The broad band between 2,800 and 3,000 cm^{-1} is characterized to the -CH stretching vibration [20]. For MA-PVA membrane (Fig. 9(b)), there is a new peak at 1,700 cm^{-1} assigned to the ester group (-C=O) in polymer matrix, demonstrating that cross-links were formed between PVA chains. For 15RHA-silica/MA-PVA membrane, the new broad band from 1,200 to 900 cm^{-1} is explained by the stretching vibration of Si-O-Si [17]. The intensity of -OH broad bands in the spectra of MA/PVA and 15RHA-silica/MA-PVA membranes is higher than in PVA membrane, which shows the increase in number of -OH, leading to better interactions between membranes and ethanol solution.

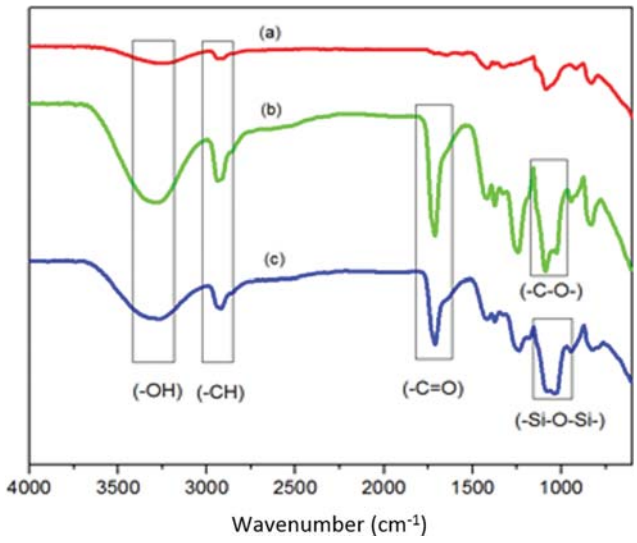

Fig. 9. FTIR spectra of (a) PVA, (b) MA-PVA, and (c) 15RHA-silica/MA-PVA membranes.

3-3. SEM Image

Fig. 10 shows SEM image of tubular ceramic-supported 15RHA-silica/MA-PVA membrane. The active layer was coated on the inside

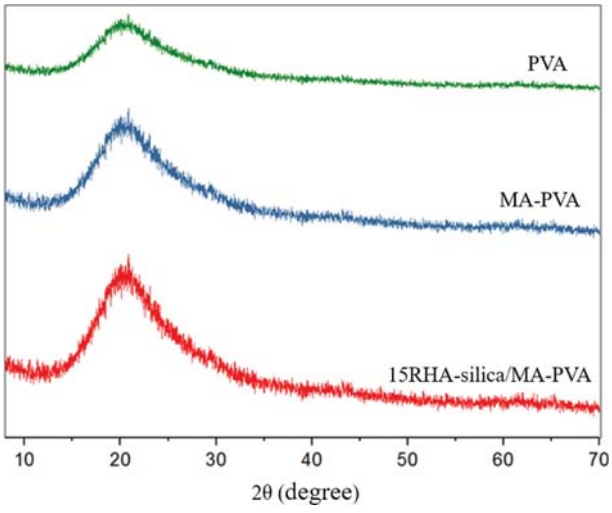

Fig. 8. XRD patterns of PVA and 15RHA-silica/MA-PVA membranes.

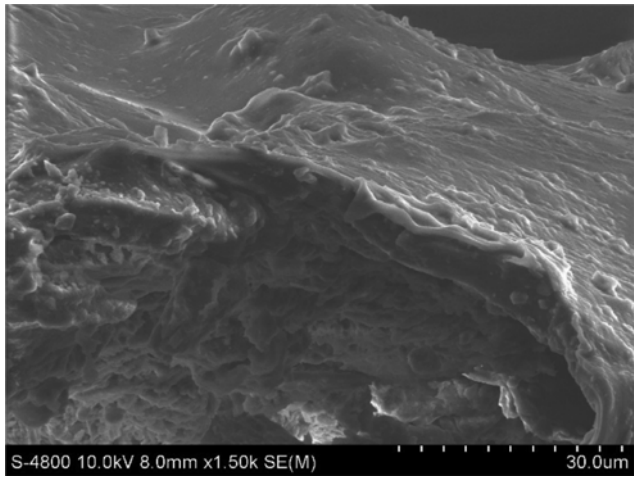

Fig. 10. SEM image of tubular ceramic-supported 15RHA-silica/MA-PVA membrane.

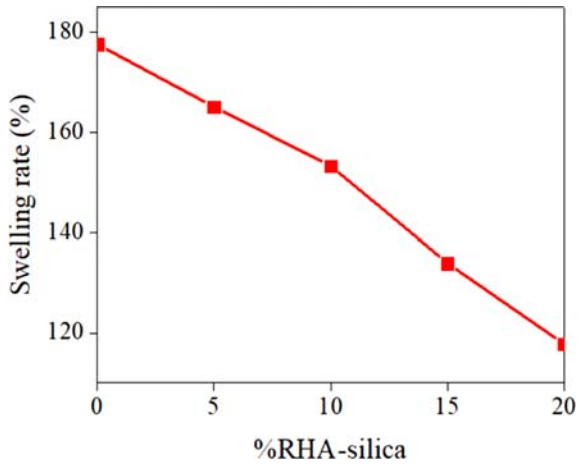

Fig. 11. Swelling rate of RHA-silica/MA-PVA membranes.

of the ceramic tube with an average thickness of 30 μm. This thickness provided high PV performance of the tubular composite membrane for the dehydration of 95 wt% ethanol solution with PSI of 3.9 kg/m^2·h.

3-4. Swelling Rate

Fig. 11 shows the swelling rate of RHA-silica/MA-PVA membranes with different RHA-silica content. The swelling rate decreases as RHA-silica content is increased. This could be explained as follows: the higher the RHA-silica content, the less hydrophilic the membrane is and hydrogen bonds between RHA-silica and PVA are formed leading to rigid polymer matrix. Thus, RHA-silica enhances the longevity of the membrane.

3-5. Contact Angle

Results of contact angle measurement of neat PVA, MA-PVA, and 15RHA-silica/MA-PVA membranes are shown in Fig. 12. The PVA membrane has a low contact angle of 53°, which is consistent with its hydrophilic property. The MA-PVA membrane has a higher contact angle of 66.4°, indicating that this membrane surface is more hydrophobic. This could be explained by the fact that -OH

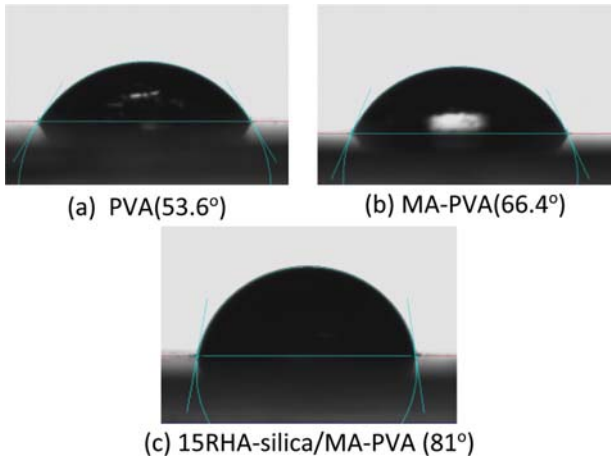

Fig. 12. Water contact angles of (a) neat PVA, (b) MA-PVA, and (c) 15RHA-silica/MA-PVA membranes.

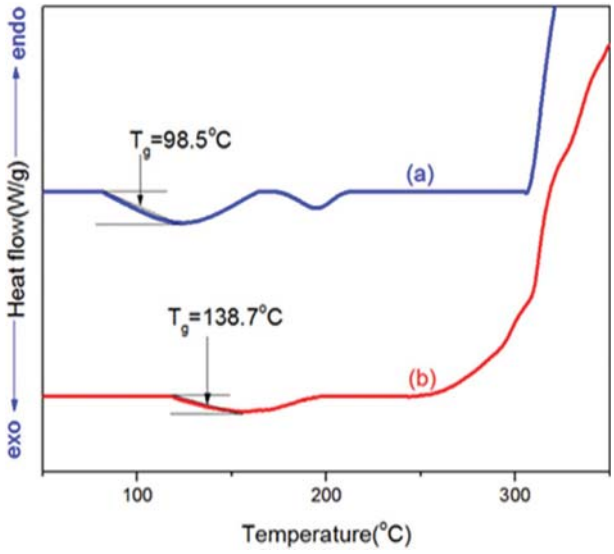

Fig. 13. DSC curves of (a) PVA and (b) 15RHA-silica/MA-PVA membranes.

groups of PVA interacted with -COOH groups of MA to form cross-links between PVA chains, resulting in the increase of hydrophobicity. The 15RHA-silica/MA-PVA membrane has the widest contact angle of 81°. The addition of RHA-silica leads to the decrease of membrane hydrophilicity, which could be explained as follows: the RHA-silica tends to form aggregation at high content (15 wt%), leading to the decrease in the number of silanol groups [12].

3-6. DSC Analysis

Fig. 13 shows that the glass transition temperature (T_g) increases with the presence of malic acid and RHA-silica in PVA polymer membrane. T_g of PVA and 15RHA-silica/MA-PVA membranes are 98.5 °C and 138.7 °C, respectively. The T_g of MA-PVA is enhanced because the carboxyl groups in MA interact with hydroxyl groups in PVA, restricting the motion of PVA molecular chains. Besides, the silanol groups of RHA-silica also interact with PVA, leading to polymer network being restricted and the increase of T_g. The DSC results revealed that thermal stability of PVA was improved by the cross-linking with MA and RHA-silica as reinforcing material.

CONCLUSIONS

Tubular ceramic-supported 15RHA-silica/MA-PVA membrane was successfully fabricated for PV dehydration of 95 wt% ethanol solution. 15RHA-silica/MA-PVA membrane exhibited high PV performance, which was higher than that of MA/PVA with the permeate flux of 0.0856 kg/m^2·h, separation factor of 46.6, and PSI of 3.9 kg/m^2·h. XRD, DSC, and swelling rate results confirmed that using RHA-silica reduced the crystalline region and the swelling rate and the membrane became more thermally stable. SEM image showed the active layer thickness of 15RHA-silica/MA-PVA membrane was 30 μm inside the ceramic support. Therefore, RHA-silica could be considered as a potential filler for fabricating the tubular ceramic-supported nanocomposite membrane to produce the anhydrous ethanol by PV.

REFERENCES

1. T. Uragami, T. Saito and T. Miyata, *Carbohydr. Polym.*, **120**, 1 (2015).
2. R. Baker, Membrane technology and applications, England, Second Edition, Wiley, 545 (2014).
3. Y. K. Ong, G. M. Shi, N. L. Le, Y. P. Tang, J. Zuo, S. P. Nunes and T. S. Chung, *Prog. Polym. Sci.*, **57**, 1 (2016).
4. K. Hunger, N. Schmeling, H. B. T.Jeazet, C. Janiak, C. Staudt and K. Kleinermanns, *Membranes*, **2**, 727 (2012).
5. L. Liu and S. E. Kentish. *J. Membr. Sci.*, **553**, 63 (2018).
6. Y. Zhu, S. Xia, G. Liu and W. Jin, *J. Membr. Sci.*, **349**, 341 (2010).
7. N. M. Kha and N. H. Hieu, 5th World Conference on Applied Sciences, Engineering & Technology, Ho Chi Minh (2016).
8. N. N. P. Duy and N. H. Hieu, *Eng. Trans.*, **56**, 1693 (2017).
9. M. Sameia, M. Iravaniniaa, T. Mohammadia and A. A. Asadibi, *Chem. Eng. Process. Process Intensif.*, **109**, 11 (2016).
10. H. Nagasawa and T. Tsuru, *Current Trends and Future Developments on (Bio-) Membranes*, 217, Elsevier (2017).
11. M. Samei, T. Mohammadi and A. A. Asadi, *Chem. Eng. Res. Des.*, **91**, 2703 (2013).
12. H. Pingan, J. Mengjun, Z. Yanyan and H. Ling, *RSC Adv.*, **7**, 2450 (2017).
13. S. Gu, J. Zhou, C. Yu, Z. Luo, Q. Wang and Z. Shi, *Ind. Crops Prod.*, **65**, 1 (2015).
14. V. R. Shelke, S. S. Bhagade and S. A. Mandavgane, *Bull. Chem. React. Eng. Catal.*, **5**, 63 (2011).
15. P. Velmurugan, J. Shim, K. J. Lee, M. Cho, S. S. Lim, S. K. Seo and B. T. Oh, *J. Ind. Eng. Chem.*, **29**, 298 (2015).
16. J. Li, C. Yang, L. Zhang and T. Ma, *J. Organomet. Chem.*, **696**(9), 1845 (2011).
17. C. N. H. Thuc and H. H. Thuc, *Nanoscale Res. Lett.*, **8**, 58 (2013).
18. E. Rafiee, S. Shahebrahimi, M. Feyzi and M. Shaterzadeh, *Int. Nano Lett.*, **2**, 29 (2012).
19. T. J. Alwan1, Z. A. Toma, M. A. Kudhier and K. M. Ziadan, *Madridge J. Nano Tec. Sci.*, **1**, 1 (2016).
20. Z. Peng, L. X. Kong, S. D. Li and P. Spiridonov, *J. Nanosci. Nanotechnol.*, **6**(12), 3934 (2006).